IOP PUBLISHING JOURNAL OF PHYSICS: CONDENSED MATTER

J. Phys.: Condens. Matter **19** (2007) 156205 (12pp) doi:10.1088/0953-8984/19/15/156205

Atomic-scale structure of nanocrystalline CeO_2–ZrO_2 oxides by total x-ray diffraction and pair distribution function analysis

Milen Gateshki[1], Markus Niederberger[2], Atul S Deshpande[2], Yang Ren[3] and Valeri Petkov[1,4]

[1] Department of Physics, Central Michigan University, Mount Pleasant, MI 48859, USA
[2] Max Planck Institute of Colloids and Interfaces, Colloid Chemistry, Research Campus Golm, D-14424 Potsdam, Germany
[3] Advanced Photon Source, Argonne National Laboratory, Argonne, IL 60439, USA

E-mail: petkov@phy.cmich.edu

Received 15 November 2006, in final form 18 February 2007
Published 16 March 2007
Online at stacks.iop.org/JPhysCM/19/156205

Abstract

Total x-ray diffraction and atomic pair distribution function analysis have been used to determine the atomic ordering in nanocrystalline (∼1.5 nm in size) CeO_2–ZrO_2 prepared by a sol–gel route. Experimental data show that the oxides are a structurally and chemically inhomogeneous mixture of nanoscale domains with cubic-type and monoclinic-type atomic ordering, predominantly occupied by Ce and Zr atomic species, respectively. The study is another demonstration of the great potential of non-traditional crystallography in studying the structure of nanocrystalline materials.

(Some figures in this article are in colour only in the electronic version)

1. Introduction

Crystalline ZrO_2–CeO_2 oxides are widely used as catalysts, solid state electrolytes, fuel cells and gas sensors [1–5]. Since properties of materials are, to a great extent, determined by their atomic-scale structure, many studies have been devoted to optimizing the useful properties of ZrO_2–CeO_2 crystals by fine-tuning their structure [1–9]. It has been found that a homogeneous distribution of Ce and Zr atoms over the crystalline lattice is beneficial to most of these materials' properties, especially the catalytic ones. Recently, attention has shifted to nanocrystalline ZrO_2–CeO_2 oxides, which show improved performance in comparison with their crystalline counterparts [1, 10]. Currently the goal is to achieve precise control over the distribution of Ce and Zr atoms inside ZrO_2–CeO_2 nanocrystals, which, in turn, requires

[4] Author to whom any correspondence should be addressed.

 © 2007 IOP Publishing Ltd Printed in the UK

good knowledge about the atomic-scale structure. Nanocrystalline materials, however, show a very limited (to a few nanometres) length of structural coherence and are difficult to study by Bragg x-ray diffraction that is routinely applied to determine the atomic-scale structure of usual (ordered over hundreds of nanometres) crystals. Here we apply a non-traditional experimental approach involving total x-ray diffraction (XRD) and atomic pair distribution function (PDF) analysis to determine the atomic-scale structure of nanocrystalline ZrO_2–CeO_2 oxides obtained by a novel wet technological route. We show that total XRD and PDF may access the structural and chemical homogeneity of nanocrystalline ZrO_2–CeO_2 in full detail, and deserve to be employed more frequently than now in nanomaterial research.

2. Experimental details

2.1. Sample preparation

Nanocrystalline $Ce_xZr_{1-x}O_2$ ($x = 0$, 0.2, 0.5, 0.7, 1) oxides were prepared from ammonium cerium nitrate $(NH_4)_2Ce(NO_3)_6$ (Aldrich, 98.5%) and zirconyl chloride $ZrOCl_2{\cdot}8H_2O$ (Riedel-de Haën, 99.5%) using the following procedure. Appropriate amounts of the precursors were dissolved together in 40 ml of distilled water. A total of 1.3–1.5 ml of a 25% aqueous NH_3 solution was added rapidly to the initial solution to raise the pH above 10, leading to co-precipitation of the metal hydroxides. A total of 5 ml of distilled water and a calculated amount of 90% HNO_3 was added to the washed precipitate. The ratio of HNO_3 to metal content was varied systematically from 1:1 for a pure CeO_2 sample to 1.5:1 for a pure ZrO_2 sample. The resultant suspension was sonicated (Elma Transsonic Digital S, 140% ultrasound power) for 45–60 min to prevent growing the crystallites beyond a certain size. During sonication, the temperature of the water bath increased to 40–50 °C. Transparent gels were obtained from these sols upon evaporation of water. Using an analytical ultracentrifugation method (Beckman Optima XL-I analytical ultracentrifuge) it was found that the thus obtained powders were almost monodisperse and very fine, with an average crystallite size of only 3 nm. More details of the preparation procedure may be found in [10].

2.2. X-ray diffraction experiments

Nanocrystalline $Ce_xZr_{1-x}O_2$ oxides were subject to XRD experiments at the beamline 11-ID-C (Advanced Photon Source, Argonne National Laboratory) using synchrotron radiation of energy 115.013 keV ($\lambda = 0.1078$ Å). Crystalline ZrO_2 and CeO_2 oxides (Z-Tech, Australia, 99.97%) were also measured and used as standards. Synchrotron radiation x-rays were employed for two reasons: first, the high flux of synchrotron radiation x-rays allowed us to measure the rather diffuse XRD patterns of $Ce_xZr_{1-x}O_2$ nanocrystals with very good statistical accuracy for relatively short data collection times. Second, the high energy of synchrotron radiation x-rays allowed us to collect data over a wide range (1–30 $Å^{-1}$) of scattering vectors Q, which is important [11, 12] for the success of the atomic PDF analysis. All samples were sealed between Capton foils and the measurements were performed in transmission geometry. Scattered radiation was collected with an imaging plate detector (mar345), except in the case of crystalline ZrO_2, when a point detector (Ge SSD) was used. Up to ten images/scans were taken for each of the samples. The corresponding images/scans were combined, subjected to geometrical corrections, integrated and reduced to one-dimensional XRD patterns shown in figure 1.

3. Results

As can be seen in figure 1, the XRD patterns of crystalline ZrO_2 and CeO_2 show well-defined Bragg peaks up to $Q \sim 12$ $Å^{-1}$, as might be expected for materials exhibiting a long-

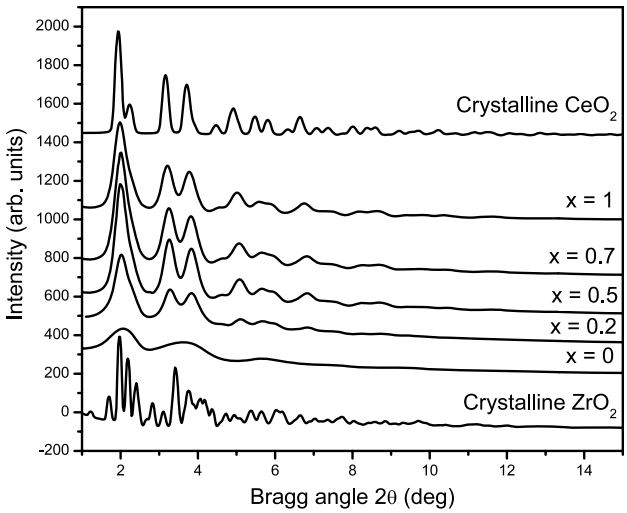

Figure 1. XRD patterns for nanocrystalline $Ce_xZr_{1-x}O_2$ ($x = 0$, 0.2, 0.5, 0.7, 1) and crystalline CeO_2 and ZrO_2 oxides. Note that the Brag peaks in the XRD pattern for crystalline ZrO_2 are somewhat better resolved than those in the XRD pattern for crystalline CeO_2 due to the fact that the point detector employed in this case had a better resolution than the imaging plate detector used to collect all other data sets.

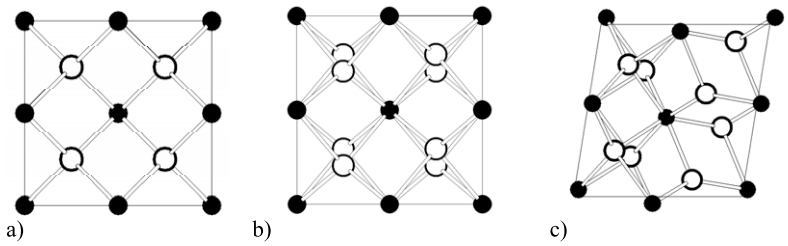

Figure 2. Fragments from the crystal structures of cubic CeO_2 (a), tetragonal $Ce_xZr_{1-x}O_2$ (b) and monoclinic ZrO_2 (c). Metal and oxygen atoms are shown as closed and open circles, respectively.

range atomic order. Such patterns lend themselves to traditional crystallographic analysis. In particular, previous crystallographic studies have determined that atoms in crystalline CeO_2 occupy the vertices of a cubic lattice of the type shown in figure 2(a). The XRD patterns of $Ce_xZr_{1-x}O_2$ nanocrystals, however, show only a few poorly defined Bragg-like peaks that merge into a slowly oscillating diffuse component at Q-values as low as 6–8 Å as usually seen with materials exhibiting a substantially limited length of structural coherence. Since the scattered intensity distribution in the XRD patterns of the nanocrystals appears similar to that in the XRD pattern of crystalline CeO_2, we attempted to analyse the experimental data for the nanocrystalline oxides in the traditional way, assuming a model based on the cubic (space group $Fm\bar{3}m$) structure of crystalline CeO_2. The presence of two metallic species in the mixed oxides was taken into account by randomly populating the cation positions in the cubic structure with Ce and Zr atoms in due proportions. The analysis was done by the Rietveld method [13, 14] with the help of the program FullProf [15]. As an example, results from the Rietveld analysis of the XRD patterns of nanocrystalline CeO_2 and $Ce_{0.2}Zr_{0.8}O_2$ are shown in figure 3.

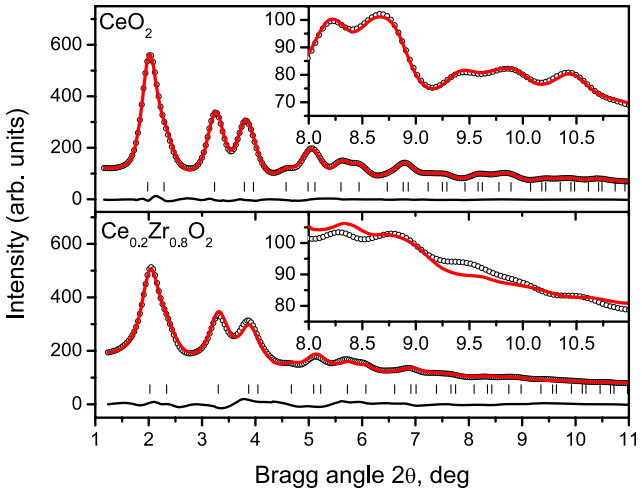

Figure 3. Experimental (symbols) and calculated (line) XRD patterns of nanocrystalline CeO_2 and $Ce_{0.2}Zr_{0.8}O_2$. The calculated patterns are derived through a Rietveld-type analysis of the experimental data using a model based on the cubic-type structure of crystalline CeO_2. The residual difference between the experimental and model data is also given in the lower part of the plots. The positions of the Bragg peaks due to the cubic structure are shown as bars.

As can be seen in the figure, the experimental XRD data for nanocrystalline CeO_2 are very well reproduced by a periodic model atomic arrangement with the structure of crystalline CeO_2. The result indicates that both nanocrystalline and crystalline CeO_2 exhibit a cubic-type structure (shown in figure 2(a)). The experimental and model data for nanocrystalline $Ce_{0.2}Zr_{0.8}O_2$ also agree, but the level of agreement is not as good as that achieved with nanocrystalline CeO_2 (see the inset in figure 3(b)). The Rietveld analyses of the XRD patterns of other mixed nanocrystalline oxides yielded similar outcomes. Further attempts to improve the Rietveld analyses failed because of the rather diffuse nature of the XRD patterns. If the Rietveld analyses, regardless of their inability to explain several low-intensity and broad features in the experimental data, are still considered successful, a conclusion may be drawn that a model featuring a cubic lattice with a random distribution of Zr and Ce atoms on its cationic positions too is a reasonably good representation of the atomic ordering in nanocrystalline $Ce_xZr_{1-x}O_2$. Such a conclusion is consistent with the observed linear dependence of the parameter of that cubic lattice on the relative Zr/Ce content (i.e. from the Vegard-type behaviour of the lattice parameter versus Zr/Ce concentration) as discussed in [10]. The conclusion implies that the nanocrystalline $Ce_xZr_{1-x}O_2$ oxides studied are structurally and chemically homogeneous at the atomic scale, i.e., as usually said, they are single-phase materials. Such a conclusion would have been unambiguous in the case of usual crystals since the sharp features (Bragg diffraction peaks) in their XRD patterns allow us to identify all distinct phases in a material, when they are present in a non-negligible (at least 1–2 vol%) amount. The situation with nanocrystalline $Ce_xZr_{1-x}O_2$ oxides is, however, more complex due to rather diffuse nature of their XRD patterns (see figure 1) and the inherent insensitivity of the traditional crystallographic studies, including Rietveld analysis, to anything else but sharp (Bragg) diffraction peaks. In fact, structural and/or chemical inhomogeneities in nanocrystals may not extend over long-range distances due to the rather limited (nano) size of the latter. Structural and/or chemical inhomogeneities (i.e. chemically and/or structurally distinct domains/phases) that extend only over a few nanometres, at most, may produce only

a low-frequency, low-amplitude (i.e. diffuse-like) contribution to the XRD patterns. Such a contribution is difficult to distinguish from the natural, slowly oscillating background (e.g. air scattering, Compton scattering, etc) that is always present in the experimental data and, as a rule, is neglected in traditional (e.g. Rietveld) crystallographic studies. Obviously an unambiguous determination of the atomic-scale structure of nanocrystals requires that all structure-relevant components of the XRD data are taken into account. This could be only done by going beyond traditional crystallography and considering the total XRD patterns, including both Bragg-like peaks (sharp features) and diffuse scattering (poorly defined features). This is indeed the essence of the total XRD and PDF data analysis approach [16–21]. For a long time the approach has been applied in structure studies of completely disordered materials such as glasses and liquids [22], and only very recently has it been applied in the structure studies of crystalline materials with intrinsic disorder [18–20, 23]. Here are the basic features of the approach, in brief. The frequently used reduced atomic PDF, $G(r)$, is defined as

$$G(r) = 4\pi r[\rho(r) - \rho_0], \tag{1}$$

where $\rho(r)$ and ρ_0 are the local and average atomic number densities, respectively, and r is the radial distance [11, 12]. As defined, the PDF $G(r)$ is a one-dimensional function that oscillates around zero and shows positive peaks at distances separating pairs of atoms, i.e. where the local atomic density exceeds the average one. The PDF $G(r)$ is a sine Fourier transform of the experimentally observable reduced structure function $F(Q) = Q[S(Q) - 1]$, i.e.,

$$G(r) = (2/\pi) \int_{Q=o}^{Q_{\max}} F(Q) \sin(Qr)\, \mathrm{d}Q, \tag{2}$$

where Q is the magnitude of the scattering vector $Q = 4\pi(\sin\theta)/\lambda$, 2θ is the angle between the incoming and outgoing x-rays and λ is the wavelength of the x-rays used. The structure function $S(Q)$ is related to the coherent part of the total XRD pattern as follows:

$$S(Q) = 1 + \left[I^{\mathrm{coh}}(Q) - \sum c_i |f_i(Q)|^2 \right] \Big/ \left| \sum c_i f_i(Q) \right|^2, \tag{3}$$

where $I^{\mathrm{coh}}(Q)$ is the coherent scattering intensity per atom in electron units and c_i and f_i are the atomic concentration and x-ray scattering factor, respectively, for the atomic species of type i [11, 12]. As can be seen from equations (1)–(3), the PDF analysis takes into account all components of the XRD data, including Bragg-like and diffuse-like scattering. Thus both the longer-range atomic order, manifested in the sharper Bragg-like peaks, and all local structural imperfections (e.g. nanoscale inhomogeneities), manifested in the diffuse-like scattering, are reflected in the experimental PDF. Also, thanks to the properties of Fourier transformation the slowly oscillating (diffuse-like scattering) components of the total XRD data appear as sharp and, hence, easily identified PDF features in real space. Furthermore, by using high-energy x-rays, high values of Q (i.e. high-order Fourier coefficients) can be assessed and, hence, fine structure features, differing in only 0.015 nm [16, 22], may be revealed. And last but not least, atomic PDFs are extracted from total XRD data already corrected for all experimental artefacts and, thus, directly give relative positions of atoms enabling convenient testing and refinement of structural models [20, 21, 23]. Experimental PDFs for nanocrystalline $Ce_xZr_{1-x}O_2$ are shown in figure 4. The processing of total XRD data and converting them to atomic PDFs was done with the help of the program RAD [24].

4. Discussion

As can be seen in figure 4, the experimental PDFs for crystalline CeO_2 and ZrO_2 are rich in well-defined structural features/peaks extending to high real-space distances, as it should

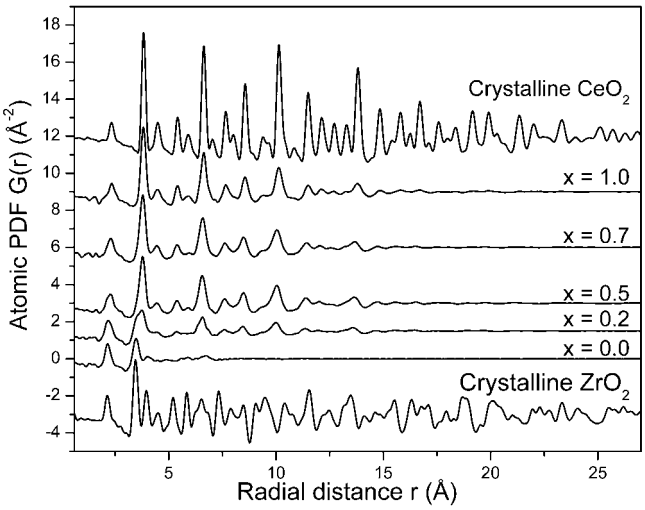

Figure 4. Experimental atomic PDFs for nanocrystalline $Ce_xZr_{1-x}O_2$ ($x = 0$, 0.2, 0.5, 0.7, 1) and crystalline CeO_2 and ZrO_2 oxides extracted from the total XRD data of figure 1.

be with materials exhibiting a long-range atomic order. The peaks reflect the presence of a well-defined and periodic sequence of coordination spheres in the crystals. The PDFs for the nanocrystalline oxides are also rich in well-defined features/peaks. These peaks are, however, broader than the ones observed in the PDFs of the crystals, reflecting the presence of a considerable local structural disorder/strain in the nanocrystals. Also, the peaks in the PDFs for nanocrystalline $Ce_xZr_{1-x}O_2$ (i.e. the sequence of distinct coordination spheres) vanish already at 10–15 Å. Obviously, these oxides, like most nanocrystalline materials, lack the extended atomic order of usual crystals. In particular, $Ce_xZr_{1-x}O_2$ nanocrystals are ordered only over distances of ≈1.5 nm that are within the average nanocrystallite size. To reveal the type of atomic ordering in $Ce_xZr_{1-x}O_2$ nanocrystals in detail we considered the corresponding atomic PDFs, starting with the first two PDF peaks, i.e. with the first and second atomic neighbour coordination spheres they reflect. This low-*r* part of the experimental PDF data is shown in figure 5.

As can be seen in the figure, the first peak in the PDFs for crystalline and nanocrystalline ZrO_2 is centred at about 2.15 Å, which is the first-neighbour Zr–O distance found in zirconia crystals. The first peak in the PDFs for both crystalline and nanocrystalline CeO_2 is centred at about 2.35 Å, which is the first-neighbour Ce–O distance found in ceria crystals. The second peak in the PDFs for crystalline and nanocrystalline ZrO_2 is centred at 3.5 Å, which is the first-neighbour Zr–Zr distance in zirconia, while that in the PDFs for crystalline and nanocrystalline CeO_2 is at 3.8 Å, which is the first-neighbour Ce–Ce distance in ceria. With the mixed nanocrystalline oxides the first two PDF peaks are doublets, reflecting the presence of two different metallic species, Zr and Ce. As expected, introducing Zr species into the CeO_2 matrix results in a gradual evolution of the position and intensity of the two components of the low-*r* PDF peaks, reflecting the appearance of Zr–O and Zr–Zr atomic pairs/distances at the expense of Ce–O and Ce–Ce ones. The position of the two components of the first peak in the experimental PDFs for $Ce_xZr_{1-x}O_2$ nanocrystals is plotted in figure 6 as a function of the relative Ce/Zr content. First-neighbour Zr–O and Ce–O distances in single-phase (i.e. structurally and chemically homogeneous) $Ce_xZr_{1-x}O_2$ crystals, as observed by extended

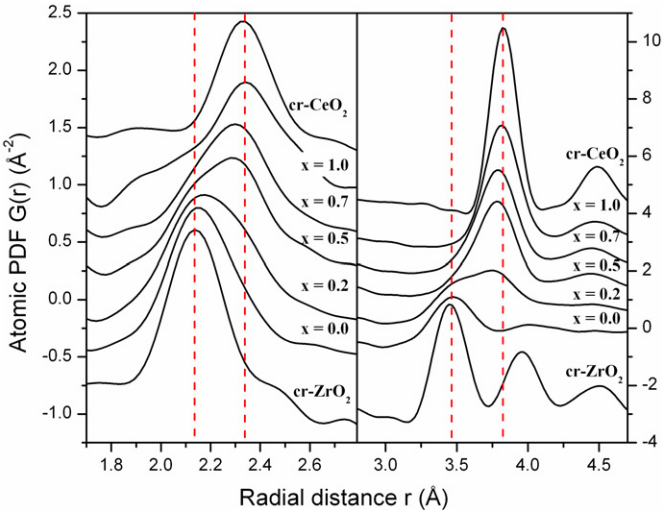

Figure 5. The first two peaks in the experimental PDFs of nanocrystalline $Ce_xZr_{1-x}O_2$ and crystalline CeO_2 and ZrO_2. The lower-r peak corresponds to first-neighbour M–oxygen distances and the higher-r peak to the M–M distances (M = Zr, Ce). Broken lines are a guide to the eye.

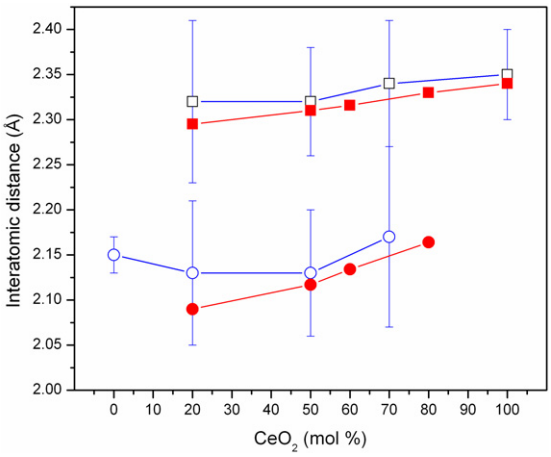

Figure 6. Positions of the two components of the first peak in the experimental PDFs for nanocrystalline $Ce_xZr_{1-x}O_2$ (open symbols: ○, □) and of Zr–O (●) and Ce–O (■) distances in single-phase $Ce_xZr_{1-x}O_2$ crystals as reported in [2].

x-ray absorption fine-structure (EXAFS) analysis [2], are also shown in the figure. As can be seen, both nanocrystalline $Ce_xZr_{1-x}O_2$ studied by us and single-phase crystalline $Ce_xZr_{1-x}O_2$ studied by others exhibit an almost identical immediate atomic ordering—that of Zr and Ce atoms coordinated to seven (bond length ∼2.15 Å) and eight oxygen atoms (bond length ∼2.35 Å), respectively. The result is in line with the findings of other recent studies [20, 25] showing that the immediate atomic ordering in $Ce_xZr_{1-x}O_2$ oxides is not much influenced by the length of structural coherence they exhibit. This is not a surprise considering the high strength of (Zr, Ce)–oxygen bonds, demonstrated by the high melting points of $Ce_xZr_{1-x}O_2$ oxides [7].

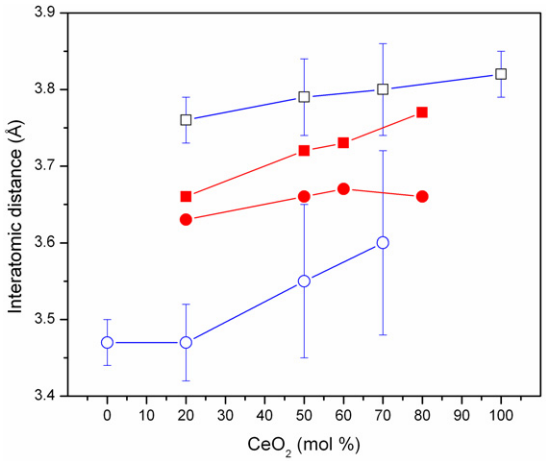

Figure 7. Positions of the two components of the second peak in the experimental PDFs for nanocrystalline $Ce_xZr_{1-x}O_2$ (open symbols: ○, □) and of Zr–Zr (●) and Zr–Ce (■) distances in single-phase $Ce_xZr_{1-x}O_2$ crystals as reported in [2].

The position of the two components of the second peak in the experimental PDFs is plotted in figure 7. First-neighbour Zr–Zr and Zr–Ce distances in single-phase $Ce_xZr_{1-x}O_2$ crystals, as observed by EXAFS studies [2], are shown in the figure as well. As can be seen, the two components of the second PDF peaks are well separated from each other in all mixed nanocrystalline oxides, remaining very close to the Zr–Zr (∼3.5 Å) and Ce–Ce (∼3.8 Å) distances found in pure ZrO_2 and CeO_2. Obviously, not only the first (metal–oxygen) coordination spheres, but also the second (metal–metal) coordination spheres of Zr and Ce do not change much in all nanocrystalline $Ce_xZr_{1-x}O_2$ oxides studied. On the other hand, the Zr–Zr and Zr–Ce first-neighbour distances in single-phase crystals are found to be practically the same (∼3.65 Å). Single-phase $Ce_xZr_{1-x}O_2$ crystals are carefully prepared to achieve a homogeneous distribution of Zr and Ce atoms over the cationic sites of the crystalline lattice [2] and, hence, most Zr atoms end up having Ce atoms as first metal neighbours, and vice versa. This could only happen when the different oxygen coordination, seven for Zr and eight for Ce, of Ce and Zr first neighbours has adjusted itself accordingly. Obviously, in single-phase $Ce_xZr_{1-x}O_2$ crystals this is achieved by the emerging of a single M–M (M = Zr, Ce) distance. The observation that Zr–Zr and Ce–Ce distances in the nanocrystalline oxides retain their substantially different values shows that such a readjustment of Zr–O and Ce–O polyhedra has not taken place in this case. This may occur when most Ce and Zr atoms end up with like atomic species as first metal neighbours, i.e. when Ce and Zr segregate at the atomic scale. Thus total XRD coupled to atomic PDF analysis, contrary to traditional crystallographic studies [10], indicate the presence of local chemical inhomogeneities in the mixed nanocrystalline $Ce_xZr_{1-x}O_2$ oxides we study. Here it is worth noting that the presence of two substantially different metal–metal distances (metal = Ce, Zr) is inconsistent with the cubic-type and tetragonal-type structures used to describe the atomic ordering in single-phase (chemically homogeneous) $Ce_xZr_{1-x}O_2$ crystals [4, 9]. If, however, one assumes that the atomic-scale structure of nanocrystalline $Ce_xZr_{1-x}O_2$ is distorted only locally to accommodate the presence of two distinct metal–metal bonds but, on average, still exhibits an orthogonal (cubic/tetragonal)-type atomic symmetry, as observed with other nanocrystalline oxides [20], then it would make sense to calculate the period of repetition (lattice parameter)

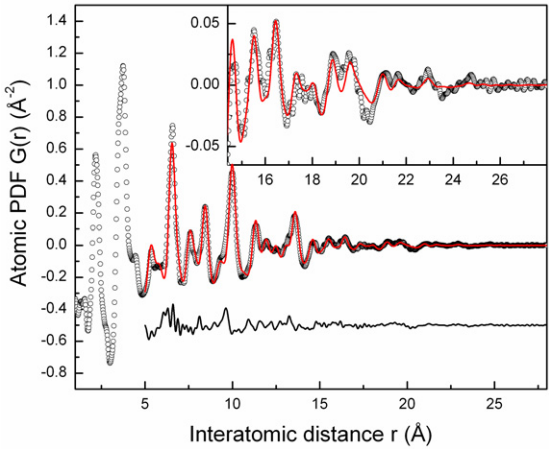

Figure 8. Fit of the high-r ($r > 5$ Å) part of the experimental PDF (dots) for nanocrystalline $Ce_{0.2}Zr_{0.8}O_2$ with a cubic (homogeneous)-type model (line). The residual difference is shown in the lower part of the plot.

of this cubic-type (on average) atomic arrangement, and see how it behaves as a function of Ce/Zr concentration. To check this assumption we fitted the experimental PDFs for the nanocrystals with a model based on the cubic-type structure shown in figure 2(a). The fit was done over a range of r-values starting from approximately 5 Å to avoid the inconsistency between the assumed uniform (i.e. a single metal–metal bond) and the real, non-uniform (two distinct metal–metal bonds) short-range atomic ordering in nanocrystalline $Ce_xZr_{1-x}O_2$ oxides. Results from the fit of the PDF for nanocrystalline $Ce_{0.2}Zr_{0.8}O_2$ are shown in figure 8, as an example. As can be seen in the figure, the high-r part of the experimental PDFs can be very well fitted with a model assuming an average atomic arrangement of a cubic type. Similar results were obtained with the other mixed nanocrystalline oxides.

The lattice parameter of the model, resulting from the PDF fits, is shown in figure 9. The lattice parameters of single-phase $Ce_xZr_{1-x}O_2$ crystals [2] and that of nanocrystalline ZrO_2, found to exhibit an average cubic-type structure [20, 25], are also shown. Note that in [2], some of the $Ce_xZr_{1-x}O_2$ crystals studied have been reported to have a structure of a tetragonal (see figure 2(b)) and not a cubic type. In these cases a 'pseudocubic' lattice parameter, a', has been calculated using the formula $a' = (2(\sqrt{2}a)+c)/3$, where a and c are the parameters of the tetragonal lattice [1]. As can be seen in figure 9, the lattice parameters of crystalline, together with those for 'pseudocubic', ZrO_2 nanocrystals, show a linear dependence on Ce/Zr content. This is the usual picture observed with single-phase materials, i.e. materials that are structurally and chemically homogeneous at the atomic scale, according to Vegard's law [26]. The lattice parameter of nanocrystalline $Ce_xZr_{1-x}O_2$ oxides with assumed locally distorted but cubic, on average, structure, however, substantially deviates from the dependence observed with homogeneous crystalline $Ce_xZr_{1-x}O_2$ oxides. This result indicates that the atomic ordering in nanocrystalline $Ce_xZr_{1-x}O_2$ oxides may not be described in terms of a locally distorted yet structurally homogeneous (i.e. a single-phase) model either. Finally, a model featuring an inhomogeneous mixture of Zr-rich and Ce-rich phases, with a length of structural coherence limited to ≈1.5 nm, where each of the metallic species keeps its preferred local coordination, a monoclinic-type (seven Zr–O bonds; see figure 2(c)) for the Zr-rich phase and cubic-type (eight Ce–O bonds; see figure 2(a)) for the Ce-rich phase, was attempted. According the model, nanocrystalline $Ce_xZr_{1-x}O_2$ ($0 < x < 1$) are a 'mixture' of nanoscale domains with different

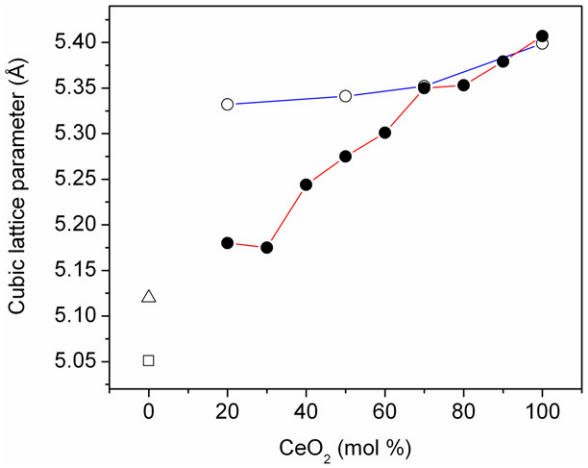

Figure 9. Lattice parameters of nanocrystalline $Ce_xZr_{1-x}O_2$ oxides (○) calculated from the higher-r part of the experimental PDFs using a structure model of an average cubic symmetry. The 'pseudocubic' (see the text) lattice parameters (●) of single-phase $Ce_xZr_{1-x}O_2$ crystals [2] and of nanocrystalline ZrO_2 (□, △) exhibiting a cubic-type structure [20, 25] are also shown for comparison.

chemistry and structure while nanocrystalline ZrO_2 ($x = 0$) and CeO_2 ($x = 1$) are 'single-phase' materials with monoclinic and cubic-type atomic-scale structures, respectively. The calculations were done with the help of the program PDFFIT [27] using literature structure data for monoclinic ZrO_2 [25] and cubic CeO_2 [9]. The limited length of structural coherence in the nanocrystallites was modelled by multiplying the model PDF data with a decaying exponent, as suggested in [28] and later implemented in [29]. The effect of the correction is to depress the PDF uniformly without changing its shape. Results from the model calculations together with the refined relative volume fractions of the two nanoscale 'phases' are shown in figure 10.

As can be seen in the figure, the 'two-phase' model reproduces the experimental PDFs very well, which is strong evidence in favour of its reliability. This is not a big surprise, since even crystalline $Ce_xZr_{1-x}O_2$, if not subject to an additional post-preparation treatment, are often found not to be single-phase materials due to the low solubility of CeO_2 in ZrO_2 and vice versa [1]. Here it may be noted that the relative volume fractions of Ce-rich (cubic-type) and Zr-rich (monoclinic-type) phases in the mixed nanocrystals (see the data reported in figure 10) are not exactly what one would expect for completely segregated materials of the same chemical composition. This may be an indication of a partial mixing of Zr and Ce atomic species. Unfortunately, the information content of the experimental PDFs does not allow a more precise estimate of this effect. Using extra data sets that are more sensitive to the type of atomic species, such as, for example, those obtained by resonant x-ray diffraction [30], would be necessary to address this possibility more accurately.

5. Conclusions

Total x-ray diffraction coupled to PDF data analysis allows one to determine the atomic-scale structure of nanocrystalline oxides, including the presence of nanoscale inhomogeneities, in detail, while traditional crystallography may fail. In particular, nanocrystalline ZrO_2 and CeO_2 oxides produced by a novel wet chemical route are found to possess monoclinic-type and cubic-

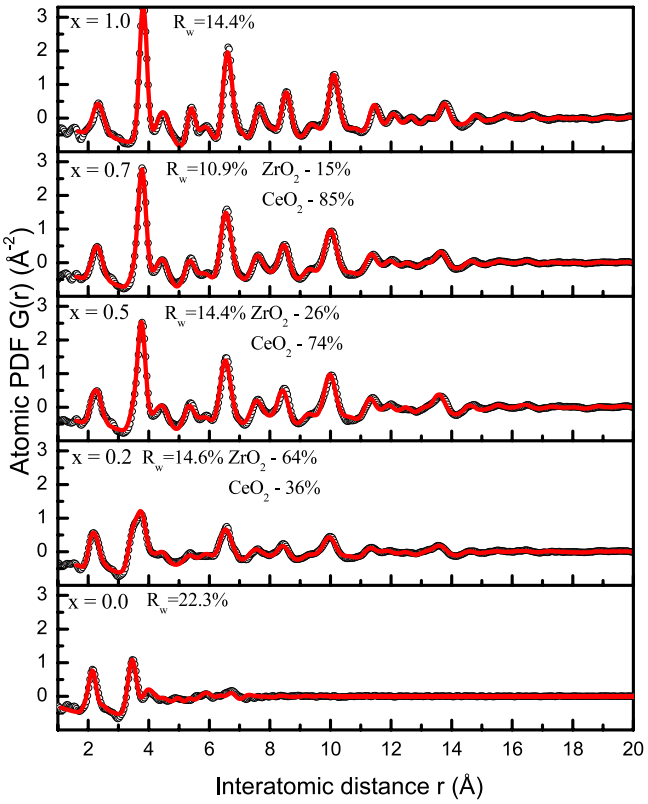

Figure 10. Experimental (symbols) and model (solid line) PDFs for nanocrystalline $Ce_xZr_{1-x}O_2$ ($x = 0.0, 0.2, 0.5, 0.7, 1.0$). The model PDFs are calculated from a 'two-phase' model described in the text. The corresponding agreement factors R_w, as defined in [20, 27], are shown by each of the fits[5].

type structures, similarly to the corresponding bulk crystals. Nanocrystalline $Ce_xZr_{1-x}O_2$ ($0 < x < 1$) oxides are a 'mixture' of Zr-rich and Ce-rich nanoscale phases/domains also of the monoclinic-type and cubic-type structure, respectively. As with the corresponding crystals, some post-preparation treatment may be needed with nanocrystalline $Ce_xZr_{1-x}O_2$ oxides obtained by wet chemical routes to achieve a more complete chemical and structural homogeneity at the nanoscale.

Acknowledgments

This work was supported by NSF through grant DMR 0304391(NIRT) and CMU through grant REF C602281. Use of the Advanced Photon Source was supported by the US Department of

[5] It may be noted that the agreement factors achieved with the PDF fits appear somewhat higher when compared to those usually resulted from the Rietveld-type fit of diffraction data in reciprocal space. This reflects the fact that the atomic PDF differs from the corresponding XRD pattern, being a quantity much more sensitive to the local atomic ordering in materials. As a result, R_w values between 10% and 20% are common for PDF fits [18–21]. The inherently higher absolute value of the goodness-of-fit factors resulting from PDF-based fits does not affect their functional purpose as a residuals quantity that must be minimized to find the best fit and as a quantity allowing one to differentiate between competing structural models.

Energy, Office of Science, Office of Basic Energy Sciences, under Contract No DE-AC02-06CH11357.

References

[1] Di Monte R and Kašpar J 2005 *J. Mater. Chem.* **15** 633
[2] Vlaic G, Di Monte R, Fornasiero P, Fonda E, Kašpar J and Graziani M 1999 *J. Catal.* **182** 378
[3] Yashima M, Sasaki S, Yamaguchi Y, Kakihana M, Yoshimura M and Mori T 1998 *Appl. Phys. Lett.* **72** 182
[4] Yashima M, Hirose T, Katano S and Suzuki Y 1995 *Phys. Rev.* B **51** 8018
[5] Mastalir A, Frank B, Szizybalski A, Soerijanto H, Deshpande A S, Niederberger M, Schomäcker R, Schlögl R and Ressler T 2005 *J. Catal.* **230** 464
[6] Yashima M and Kobayashi S 2004 *Appl. Phys. Lett.* **84** 526
[7] Yashima M, Takashina H, Kakihana M and Yoshimura M 1994 *J. Am. Ceram. Soc.* **77** 1869
[8] Yashima M, Arashi H, Kakihana M and Yoshimura M 1994 *J. Am. Ceram. Soc.* **77** 1067
[9] Lamas D G, Fuentes R O, Fábregas I O, Fernández de Rapp M E, Lascalea G E, Casanova J R, Walsöe de Reca N E and Craievich A F 2005 *J. Appl. Crystallogr.* **38** 867
[10] Deshpande A S, Pinna N, Beato P, Antonietti M and Niederberger M 2004 *Chem. Mater.* **16** 2599
[11] Klug H P and Alexander L E 1974 *X-ray Diffraction Procedures for Polycrystalline Materials* (New York: Wiley)
[12] Egami T and Billinge S J L 2003 *Underneath the Bragg Peaks. Structural Analysis of Complex Materials* (Oxford: Pergamon)
[13] Rietveld H M 1969 *J. Appl. Crystallogr.* **2** 65
[14] Young R A (ed) 1996 *The Rietveld Method* (New York: Oxford University Press)
[15] Rodríguez-Carvajal J 1993 *Physica* B **192** 55
[16] Petkov V, Jeong I-K, Chung J S, Thorpe M F, Kycia S and Billinge S J L 1999 *Phys. Rev. Lett.* **83** 4089
[17] Billinge S J L, Proffen Th, Petkov V, Sarrao J L and Kycia S 2000 *Phys. Rev.* B **62** 1203
[18] Petkov V, Gateshki M, Choi J, Gillan E G and Ren Y 2005 *J. Mater. Chem.* **15** 4654
[19] Gateshki M, Hwang S-J, Park D H, Ren Y and Petkov V 2004 *J. Phys. Chem.* B **108** 14956
[20] Gateshki M, Petkov V, Williams G, Pradhan S K and Ren Y 2005 *Phys. Rev.* B **71** 224107
[21] Petkov V, Gateshki M, Niederberger M and Ren Y 2006 *Chem. Mater.* **18** 814
[22] Petkov V, Billinge S J L, Shastri S D and Himmel B 2000 *Phys. Rev. Lett.* **85** 3436
[23] Mamontov E, Brezny R, Koranne M and Egami T 2003 *J. Phys. Chem.* B **107** 13007
[24] Petkov V 1989 *J. Appl. Crystallogr.* **22** 387
[25] Gateshki M, Petkov V, Hyeon T, Joo J, Niederberger M and Ren Y 2006 *Solid State Commun.* **138** 279
[26] Vegard L 1921 *Z. Phys.* **5** 17
[27] Proffen Th and Billinge S J L 1999 *J. Appl. Crystallogr.* **32** 572
[28] Ergun S and Schehl R R 1973 *Carbon* **11** 127
[29] Gilbert B, Huang F, Zhang H Z, Waychunas G A and Banfield J F 2004 *Science* **305** 65
[30] Fuoss P H, Eisenberger P, Warburton W K and Bienenstock A 1981 *Phys. Rev. Lett.* **46** 1537